Combustion and Flame 222 (2020) 476–489

Contents lists available at ScienceDirect

Combustion and Flame

journal homepage: www.elsevier.com/locate/combustflame

Quantification of modeling uncertainties in turbulent flames through successive dimension reduction ☆

Nana Wang [a], Qing Xie [a], Xingyu Su [b], Zhuyin Ren [a,b,*]

[a] Institute for Aero Engine, Tsinghua University, Beijing 100084, China
[b] Center for Combustion Energy, Tsinghua University, Beijing 100084, China

ARTICLE INFO

Article history:
Received 18 May 2020
Revised 12 September 2020
Accepted 14 September 2020
Available online 24 September 2020

Keywords:
Uncertainty quantification
Turbulent flame
Active subspace
Dimension reduction
Kinetic uncertainty

ABSTRACT

For turbulent flames involving intense turbulence-chemistry interaction, quantifying the uncertainty originating from the parameters of chemical kinetics and physical models leads to a more rigorous assessment of the predictability of simulations. In the present work, a successive dimension reduction framework based on the active subspace (AS) method is formulated to efficiently quantify modeling uncertainties associated with chemical kinetics, and turbulent combustion model parameters in turbulent flame simulations. The approach is demonstrated in simulating a turbulent H_2/O_2 lifted wall-jet flame. The reduction of the high-dimensional kinetic uncertainty space is first achieved through cheap surrogate autoignition tests, and a single *active* uncertain kinetic variable is identified. Then a one-dimensional active subspace of the uncertainty space consisting of such an active kinetic variable and four turbulent combustion model parameters are further identified using 25 runs of turbulent flame simulations. Finally, the probability distribution function (PDF) of the flame lift-off length is characterized through Monte Carlo simulations within a cheap response surface that is constructed within the active subspace. The components of the active subspace reveal that both chemical kinetics and turbulent mixing are critical for the flame stabilization. Further analysis shows that the uncertainty in the turbulent heat diffusion could change the dominant reactions between R1 ($H+O_2 \leftrightharpoons O+OH$) and R9 ($H+O_2 (+M) \leftrightharpoons HO_2 (+M)$) through varying the local temperature in the flame stabilization zone. In addition, comparisons of the PDFs of the flame lift-off length show that the uncertainty induced by chemical kinetics is comparable with that induced by turbulent combustion model parameters. The successive dimension reduction of uncertain physicochemical parameter space via AS enables efficient uncertainty quantification for turbulent flames, meanwhile providing insights into the controlling physiochemical processes.

1. Introduction

The simulations of turbulent combustion involve a large number of model parameters for chemical kinetics, turbulence model and combustion model etc. These parameters can be determined from theoretical derivation, experimental measurement, or even empirical analysis, which inevitably introduce uncertainty into the simulations [1,2]. Whether the models associated with uncertainties, i.e. model-form uncertainties and parametric uncertainties, can accurately reproduce the existing experiments and further be predictive for their applications in situations where experiments are difficult or expensive, remains an open question. For example, quantification for kinetic uncertainty and model-form uncertainty in turbulent flame simulations, particularly in the context of the flamelet-based large eddy simulations, has been addressed by Mueller et al. [3–5]. The present study focuses on quantifying the uncertainty originating from the large number of parameters in kinetics, turbulence and combustion models, which would lead to a more rigorous assessment of the predictability of simulations. In addition, it is important to develop analysis methods to gain insights into the governing physiochemical processes for optimization of practical combustion devices.

The forward propagation of parametric uncertainties to simulation results is one of the central steps towards addressing the above question. A classical method to conduct the uncertainty quantification (UQ) for combustion simulations is Monte Carlo (MC) that uses a large number of samples drawn from the distribution of the uncertain parameters. Each sample corresponds to a set of model parameters, and for each sample the combustion problem is evaluated once. Then the uncertainty in simulation results

☆ Submitted to **Combustion and Flame.**

* Corresponding author.
E-mail address: zhuyinren@tsinghua.edu.cn (Z. Ren).

https://doi.org/10.1016/j.combustflame.2020.09.015
0010-2180/

can be quantified through the statistics of the predictions from all of the samples. Due to slow convergence of MC, to make the uncertainty quantification be efficient, various response surface techniques have been developed to propagate the kinetics-induced uncertainty in, for example, one-dimensional laminar flame simulations [6–10] and homogeneous reactor simulations [11–13]. A non-intrusive method is adopted in most of these works while the intrusive method has also been studied [12]. Wang et al. [1] comprehensively reviewed the response surface applications in combustion simulations. The response surface techniques mainly include sensitivity analysis based method [14], artificial neural networks [15], polynomial chaos expansions [6,16], and high dimensional model representations [17], among which the latter two additionally give global sensitivity information, providing physics insight into the models. However, for quantification of modeling uncertainties in turbulent flames involving a large number of model parameters, response surface methods alone remain intractable due to not only the 'curse of dimensionality' associated with function fitting but also the high computational cost of each individual simulation.

Dimension reduction for the uncertainty space is critical to make the construction of the response surface tractable. Local sensitivity analysis and screening methods have been employed to isolate the important chemical kinetic parameters for constructing response surfaces [17–20]. Recently, active subspace (AS) method, as another dimension reduction technique, has attracted much attention in the context of uncertainty quantification. This idea was independently proposed by Russi [21] and Constantine [22], and Constantine et al. continued to develop it to be theoretically well-founded and practical for numerical implementation [23]. Instead of identifying a subset of the inputs as important, an active subspace method identifies important directions, terms as *active subspace*, in the input space. Such important directions are sets of weights that define linear combinations of the inputs, terms as *active* inputs. Subsequently, these active inputs are adopted to construct the response surface. For example, Constantine et al. [24] employed AS to exploit active directions in a seven-dimensional input space and identified one-dimensional structure in the map from seven simulation inputs to the scramjet performance. Thus a single active variable is used to construct the response surface instead of seven parameters, which greatly reduces the required simulation runs.

Since the AS method isolates inputs combinations instead of a few sensitive ones, it leads to more sufficient dimension reduction than local sensitivity analysis and screening methods. Though the principal components (PCs) in the principal component analysis (PCA) [25] are also linear combinations of the original variables, AS method is different from PCA. The PCA reduces the dimension of datasets through covariance approximation to facilitate the interpretation of such sets of data, whereas the AS identifies directions along which a quantity of interest (QoI) changes most to approximate the QoI as a function of a few active variables and thus reduce the dimension of the input space [26]. The growth of the required number of samples to compute the active subspace is moderate with increasing input dimension, which is logarithmic with a gradient-based algorithm or linear with local linear fitting [23]. Constantine et al. recently used the AS method to develop design insight [27] and applied the approach on the design of airfoil shape [28] and turbomachinery blade [29], and adopted the method to quantify the uncertainties in hypersonic flow simulations [30].

For flame simulations, Ji et al. adopted AS to identify one-dimensional active subspace within the high-dimensional kinetic parameter space for efficient uncertainty propagation in both laminar [31] and turbulent flame simulations [32]. They compared the kinetic uncertainty active subspaces computed through zero-D autoignition simulations and Cabra H_2/N_2 lifted flame [33] simulations and determined that these two sets of simulations share the same one-dimensional active subspace when the dominant physics of the QoIs is the same. Vohra et al. [34] also identified a one-dimensional active subspace for the H_2/O_2 mechanism using a proposed active subspace-based iterative strategy. They further extended the AS analysis to include uncertainties in the activation energy of the elementary reactions and initial conditions, and a one-dimensional active subspace was also observed, demonstrating the enormous potential of the AS method in applications to uncertainty propagation in complex combustion simulation systems. However, the AS method, so far, has only been applied to reduce the kinetic uncertainty space. Its application for turbulent flames with heterogeneous uncertainty parameters e.g., both chemical kinetic and physical uncertainties, have not been reported due to the high computational cost to sample the whole physiochemical uncertain parameter space.

In this work, a framework that successively reduces the dimension of physiochemical uncertainty space through the AS method is proposed for efficient quantification of modeling uncertainties in turbulent flame simulations. A few active directions in the high-dimensional kinetic uncertainty space are first identified via AS through the cheap surrogate zero/one-D simulations. Then the active subspace of the uncertain parameter space consisting of such a few active kinetic parameters and physical model parameters is further identified, followed by the quantification of modeling uncertainties for the predicted flame characteristics. Compare to the UQ only for the kinetic parameters, the proposed method extends UQ analysis to include physical parameters and thus enables the quantitative assessment of relative importance among different parts of turbulent combustion modelling. The proposed framework can be applied to quantifying the uncertainties originating from model parameters. For the structural uncertainties associated with the form of various component models, the current framework is not applicable. The framework is demonstrated with the Burrows–Kurkov (B–K) wall-jet flame simulations [35,36], with the impact of uncertainties in kinetics and physical model parameters on the prediction of flame stabilization being quantified. The controlling physiochemical process for this flame is also analyzed.

The rest of the article is organized as the following. In Section 2, the active subspace method is recalled briefly, followed by the elaboration of the proposed successive dimension reduction (SDR) framework. The B-K flame is then described along with the characterization of the uncertain physiochemical model parameters. In Section 3, results on the active subspaces for chemical kinetics alone and for uncertain kinetic-physical parameters of the flame simulations are presented. Meanwhile, the controlling physiochemical processes for the flame stabilization are analyzed, followed by quantification of modeling uncertainties. Conclusions are in Section 4.

2. Methodology

2.1. Active subspace methods

The active subspace method [23] identifies the important directions along which the QoI varies the most. Let f represent the mapping from the uncertain inputs $\mathbf{x}$ of dimension m to a QoI. For example, in the context of homogenous autoignition simulations, the inputs $\mathbf{x}$ is a random vector of the uncertain kinetic parameters and the QoI is the ignition delay time. In turbulent flame simulations, the parameters of various models, e.g. turbulence and combustion models, along with the kinetic parameters, consist of the inputs vector $\mathbf{x}$ with a given probability distribution of $\rho(\mathbf{x})$. The forward turbulent combustion simulation is the function f, which maps the model parameters to a predicted quantity of interest.

Algorithm 2.1
Compute active subspace with gradients.

1. Draw $M = \alpha\beta\log(m)$ independent samples $\{\mathbf{x}^{(1)}, \ldots, \mathbf{x}^{(M)}\}$ from the input space $\mathbf{x} \in \mathbb{R}^m$ according to $\rho(\mathbf{x})$, α is between 2 and 10.
2. For each $\mathbf{x}^{(i)}$, compute $\nabla_{\mathbf{x}} f(\mathbf{x}^{(i)})$, where $i = 1, \ldots, M$.
3. Approximate
$$\boldsymbol{C} \approx \hat{\boldsymbol{C}} = \frac{1}{M}\sum_{i=1}^{M} \nabla_{\mathbf{x}} f(\mathbf{x}^{(i)}) \nabla_{\mathbf{x}} f(\mathbf{x}^{(i)})^T,$$
where $\hat{\boldsymbol{C}}$ is the approximation of $\boldsymbol{C}$.
4. Compute the eigendecomposition $\hat{\boldsymbol{C}} = \hat{\boldsymbol{W}}\hat{\boldsymbol{\Lambda}}\hat{\boldsymbol{W}}^T$ through singular value decomposition (SVD), where the symbol $\widehat{\ }$ represents the corresponding estimated one.
5. Separate the eigenvalues and eigenvectors
$$\widehat{\Lambda} = \begin{bmatrix} \widehat{\Lambda}_1 & \\ & \widehat{\Lambda}_2 \end{bmatrix}, \quad \widehat{\boldsymbol{W}} = \begin{bmatrix} \widehat{\boldsymbol{W}}_1 & \widehat{\boldsymbol{W}}_2 \end{bmatrix},$$
where $\widehat{\Lambda}_1 = \mathrm{diag}(\widehat{\lambda}_1, \ldots, \widehat{\lambda}_n)$ and $\widehat{\Lambda}_2 = \mathrm{diag}(\widehat{\lambda}_{n+1}, \ldots, \widehat{\lambda}_m)$ with $\widehat{\lambda}_n \gg \widehat{\lambda}_{n+1}$, and $\widehat{\boldsymbol{W}}_1$ contains the first n eigenvectors, i.e. $\hat{\mathbf{w}}_1, \ldots, \hat{\mathbf{w}}_n$, and $\widehat{\boldsymbol{W}}_2$ contains the remain eigenvectors.
6. Define the active subspace as the range of the vectors in $\boldsymbol{S} = \hat{\boldsymbol{W}}_1$ and compute the corresponding *active* variable $\mathbf{y} = \hat{\boldsymbol{W}}_1^T \mathbf{x} \in \mathbb{R}^n$.

Algorithm 2.2
Compute active subspace with global linear regression.

1. Draw $N = \alpha m$ independent samples $\{\mathbf{x}^{(1)}, \ldots, \mathbf{x}^{(N)}\}$ from the input space $\mathbf{x} \in \mathbb{R}^m$ according to $\rho(\mathbf{x})$.
2. For $i = 1, \ldots, N$, run simulations to obtain $\mathbf{f} = [f_1, f_2, \ldots, f_N]^T$.
3. Estimate $\mathbf{b} = [b_1, \ldots, b_m]^T$ through ordinary least squares (OLS) regression model
$$\hat{\mathbf{b}} = \underset{\mathbf{b}}{\mathrm{argmin}} \tfrac{1}{2}\|\mathbf{c} + \boldsymbol{X}\mathbf{b} - \mathbf{f}\|_2^2$$
where $\boldsymbol{X} = [\mathbf{x}^{(1)}, \ldots, \mathbf{x}^{(N)}]^T$, $\hat{\mathbf{b}}$ is the OLS coefficients from linear regression of f to $\mathbf{x}$.
4. Compute the normalized gradient of the linear model $\hat{\mathbf{w}} = \hat{\mathbf{b}}/\|\hat{\mathbf{b}}\|$, and $\boldsymbol{S} = \hat{\mathbf{w}}$ spans the one-dimensional active subspace for $\mathbf{f}$.
5. Use the 2D sufficient summary plot SSP($f(\mathbf{x})$, $\hat{\mathbf{w}}^T\mathbf{x}$) to validate the one-dimensional structure of f's $\mathbf{x}$ space.
6. Use bootstrap method [42] to obtain an error bound on $\hat{\mathbf{w}}$ and plot the bootstrap replicates on SSP($f(\mathbf{x})$, $\hat{\mathbf{w}}^T\mathbf{x}$), providing the confidence in validation in step (5).

The most important directions in the input space can be identified by performing an eigenvalue decomposition of the covariance matrix of the gradient

$$\boldsymbol{C} = \int \nabla_{\mathbf{x}} f(\mathbf{x}) \nabla_{\mathbf{x}} f(\mathbf{x})^T \rho(\mathbf{x}) \mathrm{d}\mathbf{x} = \boldsymbol{W}\boldsymbol{\Lambda}\boldsymbol{W}^T, \tag{1}$$

where $\rho(\mathbf{x})$ is the joint probability density function of the inputs and

$$\nabla_{\mathbf{x}} f(\mathbf{x}) = \begin{bmatrix} \frac{\partial f}{\partial x_1}(\mathbf{x}) \\ \vdots \\ \frac{\partial f}{\partial x_m}(\mathbf{x}) \end{bmatrix}. \tag{2}$$

Since $\boldsymbol{C}$ is symmetric and positive semidefinite, all the eigenvalues are nonnegative and the diagonal matrix $\boldsymbol{\Lambda}$ is

$$\boldsymbol{\Lambda} = \mathrm{diag}(\lambda_1, \ldots, \lambda_m), \quad \lambda_1 \geq \cdots \geq \lambda_m \geq 0, \tag{3}$$

with the eigenvalues being sorted in descending order. Accordingly, the normalized eigenvectors $\mathbf{w}_1, \ldots, \mathbf{w}_m$ constitute the $m \times m$ orthogonal matrix $\boldsymbol{W}$. Since the mean-squared directional derivative of f with respect to the eigenvector $\mathbf{w}_i$ is equal to the corresponding eigenvalue, i.e.

$$\int \left(\nabla_{\mathbf{x}} f(\mathbf{x})^T \mathbf{w}_i\right)^2 \rho(\mathbf{x}) \mathrm{d}\mathbf{x} = \lambda_i, \quad i = 1, \ldots, m, \tag{4}$$

the eigenvalue represents how much f changes when disturbing $\mathbf{x}$ along the direction of the corresponding eigenvector. Therefore, if there is a large gap between nth and $(n+1)$th eigenvalues, i.e. $\lambda_n \gg \lambda_{n+1}$ where λ_n is the nth eigenvalue, the corresponding first n eigenvectors are the most influential directions and the remaining $m - n$ eigenvectors can be safely ignored. The *active subspace* is the space spanned by the first n eigenvectors $S = [\mathbf{w}_1, \ldots, \mathbf{w}_n]$.

If the gradient information is ready in the simulations, as is the case for zero-D autoignition tests [37], the active subspace can be estimated through the random sampling approach following Eq. (1), with $M = \alpha\beta\log(m)$ samples, where β is the number of eigenvalues to approximate and α is an oversampling factor. With the M evaluations of the gradient, a set of eigenvalues and eigenvectors as well as the subsequent active subspace are obtained via the procedure in Algorithm 2.1.

If the gradient of the QoI with respect to the input parameters is not accessible, which is quite common for complicated and expensive simulations, e.g. turbulent combustion simulations, a one-dimensional active subspace can be explored by assuming $\nabla_{\mathbf{x}} f(\mathbf{x}) \approx \mathbf{b}$. Thus $f(\mathbf{x})$ follows a global linear regression model, i.e., $f(\mathbf{x}) \approx \mathbf{c} + \mathbf{b}^T\mathbf{x}$, which has been the case for many engineering QoIs [24,32,34,38–40]. In this situation, the eigenvalue decomposition of $\hat{\boldsymbol{C}}$ is

$$\hat{\boldsymbol{C}} = \int \mathbf{b}\mathbf{b}^T \rho(\mathbf{x}) \mathrm{d}\mathbf{x} = \mathbf{b}\mathbf{b}^T = \hat{\mathbf{w}}\hat{\lambda}\hat{\mathbf{w}}^T, \tag{5}$$

where $\widehat{\lambda} = \|\mathbf{b}\|^2$, $\hat{\mathbf{w}} = \mathbf{b}/\|\mathbf{b}\|$ and the active direction $\hat{\mathbf{w}}$ is a one-dimensional subspace, identifying one important direction in the input space. The assumption of the global linear model for $f(\mathbf{x})$ respect to the inputs can be validated by the univariate trend in a sufficient summary plot which was developed by Cook [41] in the context of regression graphics. Specifically, the sufficient summary plot is a scatter plot of QoI against the linear combination of the inputs, i.e. the active variable $\hat{\mathbf{w}}^T\mathbf{x}$, which is denoted by SSP($f(\mathbf{x})$, $\hat{\mathbf{w}}^T\mathbf{x}$). The error of the computed components of the vector $\hat{\mathbf{w}}$ is estimated by using a bootstrap method [42]. The procedure of the active subspace computation with global linear regression is outlined as Algorithm 2.2.

Once the active subspace is identified, the function f can be approximated in the low dimensional subspace. Recall that f varies mostly within the active subspace and is almost constant in the remain inactive directions, a function g of the active variables $\boldsymbol{S}^T\mathbf{x}$ can be constructed to approximate f, i.e. $f(\mathbf{x}) \approx g(\boldsymbol{S}^T\mathbf{x})$. The low-dimensional response surface from the uncertainty input space to the QoI enables the uncertainty propagation and quantification for the expensive turbulent combustion simulations. At the same time, the components of the active directions are the global sensitivities with directions [43], providing the insight information for the turbulent combustion.

2.2. Successive reduction of uncertain physicochemical parameters

In turbulent flame simulations with detailed chemical kinetics, the modeling uncertainty could be from not only kinetics but also physical model parameters such as those for turbulence and combustion models. For such a large number of uncertain inputs, the required number of samples to compute the active subspace is in the order of hundreds or even thousands with Algorithm 2.1 or 2.2. Clearly, it is too expensive to run such a large number of expensive turbulent flame simulations for a UQ analysis. In this section, a successive dimension reduction (SDR) framework based on the active subspace method is formulated by taking advantage of cheap surrogate simulations for the chemical kinetics employed in the turbulent flame simulations.

Previous works [31,34] have demonstrated that the kinetic parameters of hydrocarbon mechanism in general have low-dimensional active subspaces for a wide range of thermochemical conditions. Moreover, Ji et al. [32] recently showed that for chemical kinetics, the active subspace computed through simple representative zero/one-D simulations is similar to that computed through expensive turbulent combustion simulations if the QoIs share the same physical insights. The similarity in the dominant physiochemical process can be analyzed and assured through computational diagnostic techniques such as budget analysis, chemi-

cal explosive mode analysis (CEMA) [44] and Lagrangian tracking [45,46].

Let $\boldsymbol{\xi} = [\xi_1, \ldots, \xi_{m_k}]^T$, of dimension m_k, be the normalized kinetic parameters, $\boldsymbol{\psi} = [\psi_1, \ldots, \psi_{m_p}]^T$, of dimension m_p, be the normalized physical parameters. In this study, efficient quantification of modeling uncertainties for turbulent flames is performed through the following two successive dimension-reductions of uncertain physicochemical parameters.

Step one: Reduction of the high-dimensional kinetic parameter space

(i) Extract the representative conditions from the turbulent combustion simulations and perform cheap zero/one-D surrogate simulations at these conditions. Determine the QoI in the surrogate simulations to guarantee this QoI share the same physical insights as that in the turbulent flame simulations.

(ii) Use Algorithm 2.1 to identify the active directions, i.e., $\boldsymbol{W}_{\boldsymbol{\xi},1} = [\mathbf{w}_{\boldsymbol{\xi},1}, \ldots, \mathbf{w}_{\boldsymbol{\xi},n_k}]$, in the kinetic parameter space, for the QoI determined in *step one* (i), where n_k is the dimension of the active subspace. Note that $\boldsymbol{W}_{\boldsymbol{\xi},1}$ is of dimension $m_k \times n_k$.

(iii) Project $\boldsymbol{\xi}$ onto the active subspace spanned by the column-vectors in $\boldsymbol{W}_{\boldsymbol{\xi},1}$, i.e. $\mathbf{W}_{\boldsymbol{\xi},1}^T\boldsymbol{\xi}$, to lump the kinetic parameters to a few *active* kinetic parameters $\mathbf{w}_{\boldsymbol{\xi},1}^T\boldsymbol{\xi}, \ldots, \mathbf{w}_{\boldsymbol{\xi},n_k}^T\boldsymbol{\xi}$. As a result, the m_k uncertain kinetic parameters are condensed into n_k active ones, where m_k is dozens to thousands while n_k is typically one to five for hydrocarbon fuels [31], leading to a substantial dimension reduction of the high-dimensional kinetic parameter space.

Step two: Reduction of the active kinetic-physical parameter space

(i) Combine the n_k active kinetic parameters, i.e., $\mathbf{w}_{\boldsymbol{\xi},1}^T\boldsymbol{\xi}, \ldots, \mathbf{w}_{\boldsymbol{\xi},n_k}^T\boldsymbol{\xi}$, with the m_p physical parameters, i.e., $\psi_1, \ldots \psi_{m_p}$, to form the new uncertainty inputs $\boldsymbol{\theta} = [\mathbf{w}_{\boldsymbol{\xi},1}^T\boldsymbol{\xi}, \ldots, \mathbf{w}_{\boldsymbol{\xi},n_k}^T\boldsymbol{\xi}, \psi_1, \ldots \psi_{m_p}]^T$. Note that the dimension of the new input space is $n_k + m_p$. The required turbulent flame simulations for computing the active subspace in the new input space is $N = \alpha(n_k + m_p)$, instead of $\alpha(m_k + m_p)$ due to the reduction for the large number of the kinetics inputs.

(ii) Compute the active directions $\mathbf{W}_{\boldsymbol{\theta},1} = [\mathbf{w}_{\boldsymbol{\theta},1}, \ldots, \mathbf{w}_{\boldsymbol{\theta},n_{tot}}]$ for the QoI of turbulent combustion simulations. Note that $\boldsymbol{w}_{\boldsymbol{\theta},\mathbf{1}}$ is of dimension $(n_k + m_p) \times n_{tot}$, and n_{tot} is the few number of active directions. As a result, the effective dimension of the input parameter space has been reduced from $m_k + m_p$ to $n_k + m_p$, and eventually to n_{tot} after the successive reduction.

(iii) Construct a response surface mapping the inputs to the QoI within the successively reduced subspace to enable the otherwise intractable UQ analysis for the turbulent combustion simulations. Meanwhile, the components of active directions $\mathbf{w}_{\boldsymbol{\theta},1}, \ldots, \mathbf{w}_{\boldsymbol{\theta},n_{tot}}$ indicate the relative importance of the input parameters and the corresponding kinetic-physical processes.

It is worth mentioning that mechanism reduction, particularly for large hydrocarbon fuels, could be carried out as a preliminary step of *step one* to reduce the computational cost of the active subspace analysis for the kinetic parameters. Through mechanism reduction, the number of involved reactions for UQ analysis can be reduced by eliminating unimportant reactions. Note that mechanism reduction is different from the AS dimension reduction. For AS, the full set of reactions are maintained and the inactive subspace is removed by identifying directions along which the QoI changes most and thus reducing the dimension of the input space [23].

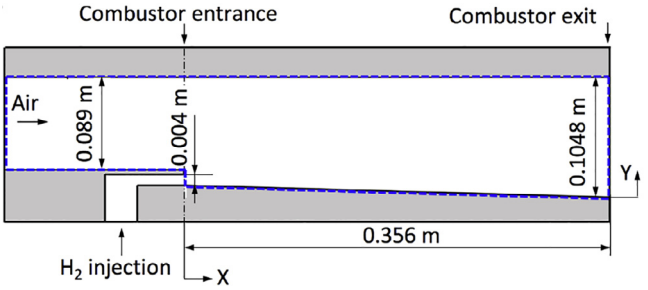

Fig. 1. The schematic of the Burrows–Kurkov combustor with the dashed-line showing the computational domain.

2.3. Demonstration case: Burrows–Kurkov H_2/O_2 wall-jet flame

The Burrows–Kurkov (B–K) wall-jet flame [35,36] is simulated with uncertainty associated with kinetics and physical models, to demonstrate the proposed SDR framework. The schematic of the B-K combustor is illustrated in Fig. 1. The high-temperature vitiated air flows through a wind tunnel into a stepped-wall combustor, while the hydrogen is injected from a slot vertical to the tunnel and then flows parallel into the vitiated airstream. The two inflowing streams, as listed in Table 1, mix with each other in the combustor, and ignition occurs downstream near the wall resulting in a wall-jet flame.

All the simulations are performed over a 2D computational domain (the dashed-line region in Fig. 1) with a compressible multi-component solver within the OpenFOAM platform [47]. The simulation details including the physical models, numerical settings and grid independence are presented in Appendix A and are summarized in Table 2. The detailed mechanism employed is the Li-2004 [48] mechanism, which consists of 9 species and 21 elementary reactions.

The simulation results are validated against experimental measurement. As shown in Fig. 2a, the flame is stabilized at around 0.17 m downstream of the fuel inlet, which is in the range of 0.15–0.2 m obtained from ultraviolet imaging [36]. Together with the contour plot, the profiles of the heat release rate (HRR) and OH mass fraction along the upper lip-line of the fuel inlet are shown in Fig. 2b. The location of the HRR peak captures the flame stabilization location better than that of the OH peak. Hence, a flame lift-off length, denoted by L, is defined by the distance from the fuel inlet to the location of the HRR peak. As shown, L is 0.174 m according to the definition. In addition, as shown in Fig. 2c, the predicted species profiles at the combustor exit agree well with the experimental ones, even though for $Y < 0.015$ m species H_2O is slightly over-predicted, and species H_2 is slightly under-predicted. The validation indicates that the model strategy adopted is adequate for the following uncertainty analysis.

In this study, the lift-off length is selected as the quantity of interest to demonstrate the proposed method for uncertainty quantification, since flame stabilization is of primary importance in practice. Moreover, the flame lift-off length is measured in the Burrows–Kurkov experiment together with an uncertainty range. This will facilitate the validation of the underlying turbulent combustion models.

2.4. Characterization of model uncertainties

For the rth reaction in Li mechanism [48], the rate-constant k_r is assumed to follow the Arrhenius rate law as a function of tem-

Table 1
The inflowing conditions for the Burrow–Kurkov experiments.

Parameter	Ma	T (K)	P (Pa)	Y_{O2}	Y_{N2}	Y_{H2O}	Y_{H2}
Air stream	2.4	1260	101,325	0.258	0.486	0.256	0.0
Hydrogen stream	1.0	254	101,325	0.0	0.0	0.0	1.0

Table 2
The simulation settings for the Burrows–Kurkov flame.

Solver	Unsteady compressible reactive flow solver
Turbulence model	Standard k-ε model with $C_\mu = 0.09$, $C_{\varepsilon 1} = 1.44$, $C_{\varepsilon 2} = 1.92$, $C_{\varepsilon 3} = -0.33$, $\alpha_k = 1.0$, and $\alpha_\varepsilon = 0.769$
Turbulence combustion model	Partially stirred reactor (PaSR) with $\tau_{mix} = k/(\varepsilon c_{flow})$, $c_{flow} = 4.0$
Turbulent transport	$Sc_t = 0.6$, $Pr_t = 0.9$
Wall treatment	The law of the wall $u^+ = \frac{1}{A}\ln(y^+) + B$ with $A = 0.4187$, $B = 5.45$

Table 3
The uncertainty factors for elementary reactions in the Li mechanism.

#	Reaction	F_r
R1	$H + O_2 \leftrightharpoons O + OH$	1.5
R2	$O + H_2 \leftrightharpoons H + OH$	1.3
R3	$H_2 + OH \leftrightharpoons H_2O + H$	2
R4	$O + H_2O \leftrightharpoons OH + OH$	1.5
R5	$H_2 + M \leftrightharpoons H + H + M$	2
R6	$O + O + M \leftrightharpoons O_2 + M$	2
R7	$O + H + M \leftrightharpoons OH + M$	3
R8	$H + OH + M \leftrightharpoons H_2O + M$	2
R9	$H + O_2 (+ M) \leftrightharpoons HO_2 (+ M)$	1.2
R10	$HO_2 + H \leftrightharpoons H_2 + O_2$	2
R11	$HO_2 + H \leftrightharpoons OH + OH$	3
R12	$HO_2 + O \leftrightharpoons O_2 + OH$	1.2
R13	$HO_2 + OH \leftrightharpoons H_2O + O_2$	3
R14	$HO_2 + HO_2 \leftrightharpoons H_2O_2 + O_2$	2.5
R15	$HO_2 + HO_2 \leftrightharpoons H_2O_2 + O_2$	1.4
R16	$H_2O_2 (+ M) \leftrightharpoons OH + OH (+ M)$	2.5
R17	$H_2O_2 + H \leftrightharpoons H_2O + OH$	3
R18	$H_2O_2 + H \leftrightharpoons HO_2 + H_2$	2
R19	$H_2O_2 + O \leftrightharpoons OH + HO_2$	3
R20	$H_2O_2 + OH \leftrightharpoons HO_2 + H_2O$	2
R21	$H_2O_2 + OH \leftrightharpoons HO_2 + H_2O$	2

perature

$$k_r(T) = A_r T^{n_r} \exp\left(-\frac{E_{a,r}}{RT}\right), r = 1, \ldots, 21, \tag{6}$$

where A_r is the pre-exponent, n_r is the temperature exponent, $E_{a,r}$ is the activation energy. This expression can be interpreted in a logarithmic form

$$\ln k_r = \ln A_r + n_r \ln T - \frac{E_{a,r}}{RT}. \tag{7}$$

Following the previous work [6,9,10,31,32,49], the rate-constants are uncertain. Specifically, the $\ln k_r$'s of all the reactions are independent of each other and normally distributed, i.e., $\ln k_r \sim \mathcal{N}(\mu, \sigma^2)$, where μ is the mean value and σ is the standard deviation. In this work, the mean of $\ln k_r$ is the corresponding nominal value $\ln k_{r0}$ and the standard deviation is set to be $\frac{1}{3}\ln F_r$, where F_r is the temperature-independent uncertainty factor adopted from Konnov [50]. The F_r's are summarized in Table 3 for all the reactions. Each $\ln k_r$ can be centered by the mean and normalized by the standard deviation as ξ_r, which follows the standard normal distribution, i.e.,

$$\xi_r = \frac{\ln k_r/k_{r0}}{\frac{1}{3}\ln F_r} \sim \mathcal{N}(0, 1), \ r = 1, \ldots, 21. \tag{8}$$

Hence, the number of the uncertain kinetic parameters is 21 and the uncertainty inputs can be represented by a 21-dimensional random vector $\xi = [\xi_1, \ldots, \xi_{21}]^T \sim \mathcal{N}(0, \mathbf{I}_{21})$.

For the turbulence and combustion models, the k-ε turbulence model parameter $C_{\varepsilon 1}$, the PaSR combustion model parameter c_{flow}, turbulent Schmidt number Sc_t and Prandtl number Pr_t are considered to be uncertain to represent the significance of turbulence, combustion, turbulent mixing modeling, respectively. The ranges from these parameters are compiled based on the reported values in literature. The uncertainty characterization of the four physical model parameters are summarized in Table 4, with uniform

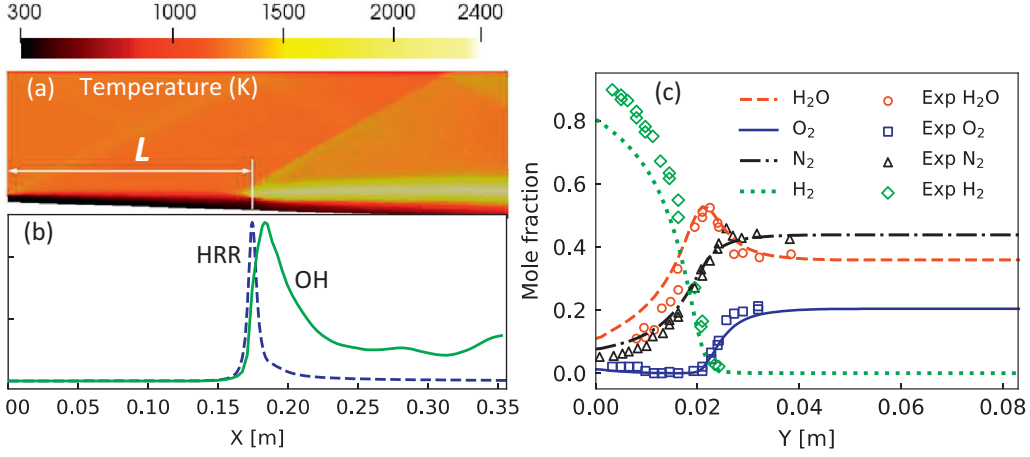

Fig. 2. (a) The contour plot of the temperature where L denotes the lift-off length, (b) the profiles of the HRR and OH mole fraction along the upper lip-line of the hydrogen inlet, and (c) the profiles of species mole fractions at the combustor exit with the experimental data.

Table 4
Uncertainty characterization of turbulence and combustion model parameters.

Parameter	Nominal	Min	Max
$C_{\varepsilon 1}$	1.44	1.3	1.7
c_{flow}	4.0	0.5	4.0
Sc_t	0.6	0.5	1.0
Pr_t	0.9	0.5	1.0

distribution on their spaces bounded by the range following the maximum entropy principle from Jaynes [51]. The turbulence model constants $C_{\varepsilon 1}$ in general has strong impact on jet spreading [52]. In addition, $C_{\varepsilon 1}$ was introduced to account for the pressure diffusion and effect of the near-wall anisotropy that may be significant in the wall-jet flame. For PaSR combustion model, the model constant c_{flow} has an impact on the mean chemical reaction rate and treated as an uncertain parameter with the range of 0.5–4.0 to account for the effects of finite rate chemistry. The parameters Sc_t and Pr_t in general have profound influence on the predicted flame characteristics through affecting turbulent mass or thermal diffusion [53,54] and a range of 0.5–1.0 is chosen according to the literature investigation. It is worth to mention that the input parameters are centered at zero and normalized to be over $[-1,\ 1]$ in the subsequent active subspace analysis, and $\langle C_{\varepsilon 1}\rangle$, $\langle c_{flow}\rangle$, $\langle Sc_t\rangle$, $\langle Pr_t\rangle$ are used to denote the corresponding normalized value.

3. Results and discussions

For the UQ analysis of expensive turbulent combustion simulations with high-dimensional uncertainty space, the aim is to propagate uncertainties in the following modeling parameters to the flame lift-off length L in the B-K simulations: (i) rate-constants $k_i's$ for the chemical kinetics, and (ii) turbulence Schmidt number Sc_t, turbulence Prandtl number Pr_t, turbulence model constant $C_{\varepsilon 1}$ and combustion model parameter c_{flow} for the physical models. The dimension of the uncertainty space is reduced within the proposed SDR framework to enable the otherwise intractable UQ. In this section, the results from implementing this heuristic approach in the B-K simulations will be demonstrated.

3.1. Active subspace of chemical kinetics and key reactions

3.1.1. Active subspace from surrogate zero-D autoignition tests

According to *step one* of the SDR framework, the active subspace of the kinetic uncertainty space is first computed through cheap surrogate simulations at the representative conditions. Previous analysis [55] showed that for the Burrows–Kurkov flame, a chemical explosive mode exists at the flame onset location, and the dominant physiochemical process for flame stabilization is autoignition. Hence, zero-D autoignition tests are chosen as the surrogate simulations. The representative condition is extracted from a critical location upstream where the ignition occurs. The critical location is defined as where the mass fraction of H_2O starts to be significantly larger than that of O_2, and recall that these two species have the almost same mass fraction in the vitiated air stream. To capture this location, the profiles of species mass fraction and temperature are plotted over the upper lip-line of the fuel inlet, as shown in Fig. 3 from which the representative condition is obtained, that species mass fractions are $Y_{H2} = 0.0191$, $Y_{O2} = 0.245$, $Y_{H2O} = 0.245$ and $Y_{N2} = 0.475$, and temperature is 956 K and pressure is 100,523 Pa. The adiabatic, isobaric autoignition tests under the representative condition as the initial state are performed based on Cantera [56].

The active subspace is computed using Algorithm 2.1 through $M = 670$ random samples drawn for the normalized rate-constants

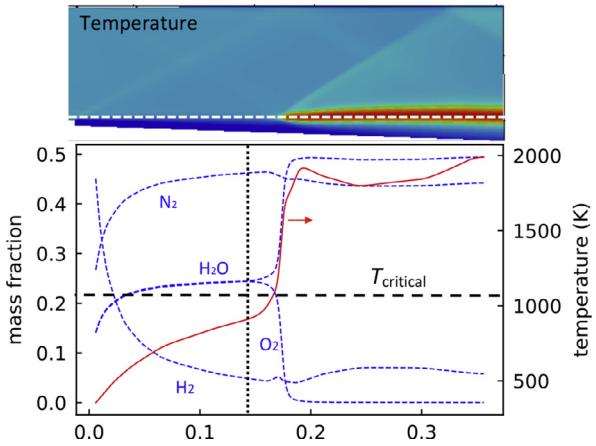

Fig. 3. The profiles of species mass fraction and temperature over the upper lip-line (the dashed line in the contour plot), and the vertical dotted line is the location where the representative condition is extracted.

$\{\xi_1, \ldots, \xi_{21}\}$ according to their distribution densities. The eigenvalues of the covariance matrix of the gradient of ignition delay time (IDT) with respect to $\boldsymbol{\theta}$ are plotted in Fig. 4a, showing that the first eigenvalue is larger than the second one by one order of magnitude, implying that the kinetics input space has a one-dimensional active subspace. To confirm this, the summary plot of log(IDT) versus $\mathbf{w}_{\boldsymbol{\xi},1}^T\boldsymbol{\xi}$ is shown in Fig. 4b, where $\mathbf{w}_{\boldsymbol{\xi},1}$ is the first eigenvector corresponding to the largest eigenvalue. As illustrated, the values of log(IDT) approximately distribute on a one-dimensional curve and the width of the curve is small, confirming the one-dimensional structure of the kinetic uncertainty space. Therefore, it is sufficient to choose the first eigenvector, i.e. $\mathbf{w}_{\boldsymbol{\xi},1}$ to span the one-dimensional active subspace for kinetic parameters.

A response surface is constructed in the active subspace by the second order polynomial fitting, as shown in Fig 4b. The probability distribution function (PDF) of the log(IDT) is subsequently evaluated via the response surface, as shown by the solid line in Fig. 4c. Meanwhile, a deterministic solution for the distribution of the log(IDT) is available by directly evaluating each sample via autoignition integration, as shown by the dashed line in Fig. 4c. As illustrated, the results from the AS method agree well with the accurate ones with the differences in the mean and standard deviation being less than 1%, demonstrating the effectivity of the AS method and the adequacy of the one-dimensional active direction $\mathbf{w}_{\boldsymbol{\xi},1}$.

The components of $\mathbf{w}_{\boldsymbol{\xi},1}$ are shown in Fig. 5, providing the relative importance of the reactions. As shown, the most sensitive reaction is R1 ($H+O_2 \leftrightharpoons O+OH$), which is the major chain branching reaction. This is consistent with the findings in the work of Wu et al. [47] that the evolutions of the OH and H radicals dominate the chemical explosive mixing layers ahead of the flame stabilization location. The secondary sensitive reaction is R9 ($H + O_2$ (+M) $\leftrightharpoons HO_2$ (+M)) which is the main competition reaction to R1 in consuming H, and no surprise it has an opposite sign to R1 and retards autoignition process.

The active subspace is also estimated with Algorithm 2.2 to confirm that it is adequate to use linear regression to compute the active subspace, since it is computationally intractable to evaluate the gradient of the flame lift-off length L through the B-K simulations and Algorithm 2.2 will be employed at this situation. The same set of samples is used to perform the calculation, and the active subspace is shown in Fig. 5 with the triangle which is in perfect consistency with that estimated based on gradient. Moreover, the overlap between the two corresponding SSPs(log(IDT),$\mathbf{w}_{\boldsymbol{\xi},1}^T\boldsymbol{\xi}$)

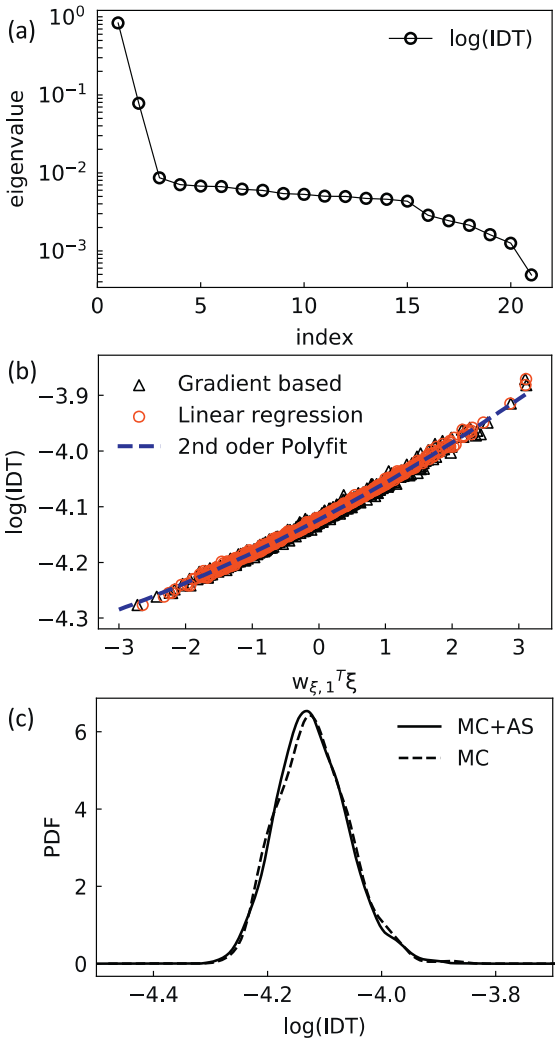

Fig. 4. (a) The eigenvalues of the covariance matrix of the gradient of IDT with respect to $\boldsymbol{\xi}$, (b) the summary plot of log(IDT) versus $\mathbf{w}_{\boldsymbol{\xi},1}^T\boldsymbol{\xi}$ from the gradient-based algorithm and linear regression, and (c) the PDFs of log(IDT).

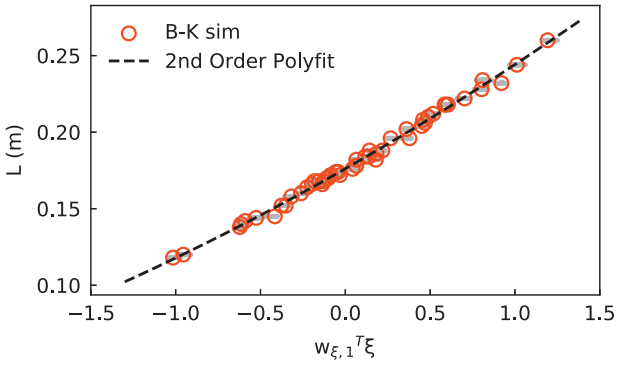

Fig. 6. The summary plot of flame lift-off length L versus $\mathbf{w}_{\boldsymbol{\xi},1}^T\boldsymbol{\xi}$ through B-K simulations; the overlapping grey dots are from 100 bootstrap replicates of SSP(L,$\mathbf{w}_{\boldsymbol{\xi},1}^T\boldsymbol{\xi}$); the dashed line is the fitted response surface by using second order ploylit.

shown in Fig. 4b demonstrates that the one-dimensional active subspaces computed by both algorithm variants coincide.

3.1.2. Assessment of active subspace with flame simulations

To assess the capacity of the surrogate simulations in computing active subspace for kinetics, the subspace is also computed using 50 B-K simulation samples to draw the comparison. The one-dimensional active direction for the flame lift-off length L computed with Algorithm 2.2 is shown in Fig. 5 with the errors estimated by bootstrap. The corresponding summary plot is displayed in Fig. 6 which shows a strong univariate trend in the function of L versus $\mathbf{w}_{\boldsymbol{\xi},1}^T\boldsymbol{\xi}$ with a narrow scatter of the 50 simples. This confirms that the kinetic uncertainty space has a one-dimensional active subspace for the QoI, which is consistent with the analysis by using the surrogate simulations.

The comparison between the active subspaces for the IDT in the autoignition simulations and the flame lift-off length L in the B-K simulations is shown in Fig. 5. As shown, these two sets of components are consistent in general. Significant differences can only be observed for the chain propagating reaction (R3). The sensitivity analysis in Li et al. [48] demonstrated that the laminar flame speed is sensitive to this reaction, while the ignition delay time is

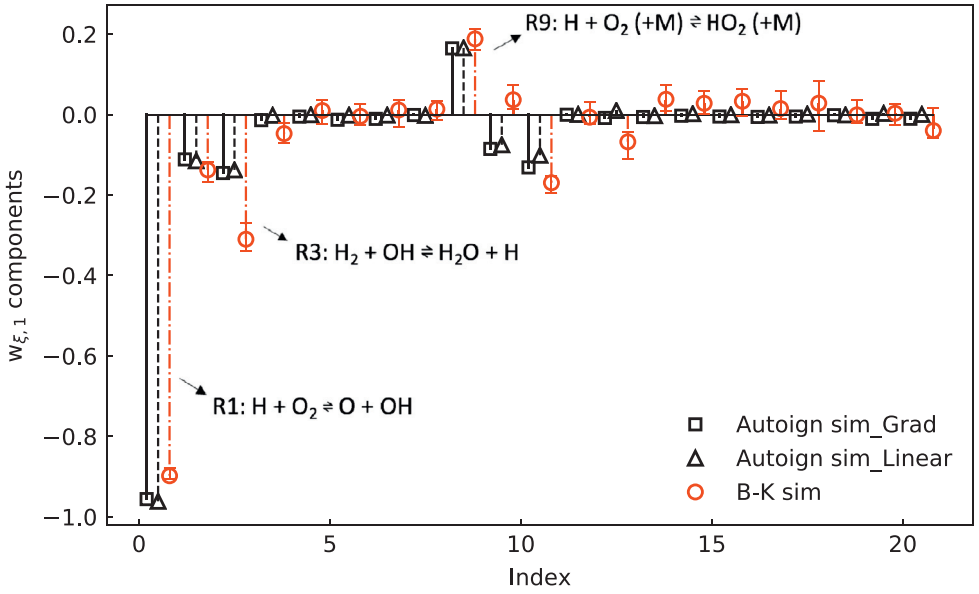

Fig. 5. The components of the active subspace computed based on gradient, linear regression through autoignition simulations for the kinetics inputs, compared with those obtained through B-K simulations.

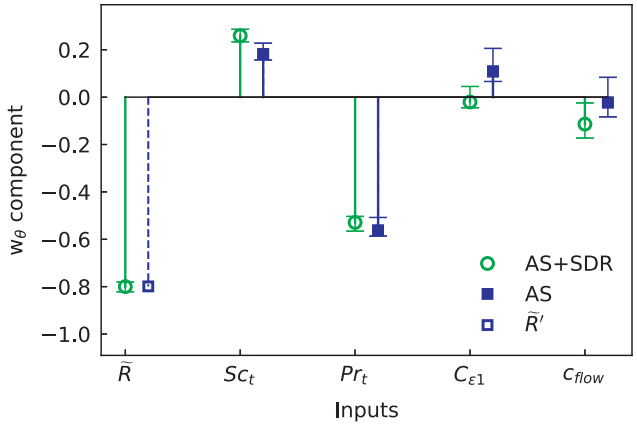

Fig. 7. The components of the active subspace $\mathbf{w}_\theta$ computed with and without the SDR framework, with the error bars estimated by bootstrap, also shown is the equivalent active rate-constant $\tilde{R}'$.

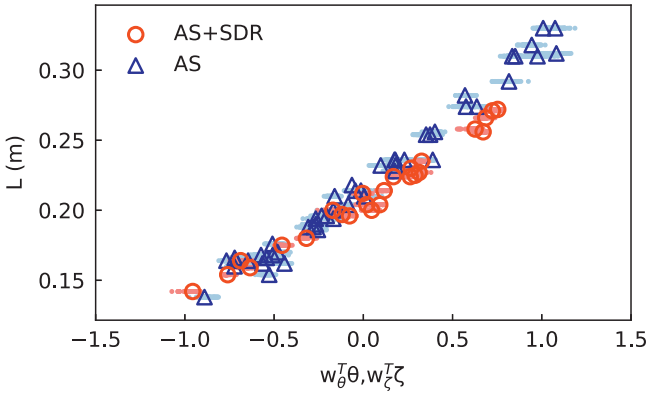

Fig. 8. The summary plot of flame lift-off length L with and without the SDR framework through B-K simulations; the overlapping dots are from 100 bootstrap replicates of the corresponding SSPs.

essentially insensitive to R3 at all conditions. This may explain the significantly promoted sensitivity of L to R3 in the B-K simulation, in which rather than a pure autoignition process, the species diffusion ahead of the flame stabilization zone elevates the reactivity of R3 and moves the lifted flame towards upstream. The sensitivity to the reaction R11 is slightly promoted for the same reason and the sensitivity to the reaction R1 is inhibited. Nevertheless, the active subspace estimated through the surrogate autoignition simulations is reasonably coincident with that computed through the B-K simulations with an inner product of 0.967. Therefore, the zero-D autoignition simulations have the ability to surrogate the expensive B-K simulations to identify the active subspace of the kinetic uncertainty space, which would significantly reduce the number of required runs in the subsequent active subspace analysis for the B-K flame involving both kinetic and physical uncertain parameters.

Following *step one* (iii) of the SDR framework, with the one-dimensional active subspace demonstrated by the surrogate simulations, an active variable is obtained by projecting the 21 rate-constants $\boldsymbol{\xi} = [\xi_1, \ldots, \xi_{21}]^T$ onto the active direction, i.e. $\mathbf{w}_{\boldsymbol{\xi},1}^T\boldsymbol{\xi}$ which can be treated as an averaged rate-constant weighted by the corresponding components of the vector $\mathbf{w}_{\boldsymbol{\xi},1}$. To make this active variable have a physical meaning that larger value represents a higher reaction rate, an *active* rate-constant, denoted by $\tilde{R}$, is defined as $-\mathbf{w}_{\boldsymbol{\xi},1}^T\boldsymbol{\xi}$, since $\mathbf{w}_{\boldsymbol{\xi},1}$ is calculated from IDTs which has a negative correlation with the reactivity. Since $\xi_i$has been normalized to follow the standard normal distribution, $\tilde{R}$ also follows the standard normal distribution, i.e. $\tilde{R} \sim \mathcal{N}(0, 1)$. This active rate-constant $\tilde{R}$ will be adopted in the later section to draw random samples from the kinetic uncertainty space and to represent the behavior of the kinetics in the B-K flames.

3.2. Dimension reduction for kinetic-physical uncertainty parameters

3.2.1. Active subspace for flame-lift off length

Lumping the active rate-constant $\tilde{R}$ and uncertain model parameters, i.e. Sc_t, Pr_t, $C_{\varepsilon 1}$ and c_{flow}, an input parameter vector represented by $\boldsymbol{\theta} = [\tilde{R}, \langle Sc_t\rangle, \langle Pr_t\rangle, \langle C_{\varepsilon 1}\ \rangle,\ \langle c_{flow}\rangle]^T \in \mathbb{R}^5$ is constructed. Following *step two* of the SDR framework, the active subspace of such a kinetic-physical input parameter space for the flame lift-off length L is explored with Algorithm 2.2 to further reduce the dimension. $N = 25$ samples with the oversampling factor being 5 is drawn from the uncertainty space spanned by $\boldsymbol{\theta}$. The R-square of the global linear regression is 0.976, suggesting that Algorithm 2.2 is adequate to identify the active subspace. The one-dimension active subspace for L is shown in Fig. 7 with the errors estimated by bootstrap. The corresponding SSP(L, $\mathbf{w}_{\boldsymbol{\theta}}^T\boldsymbol{\theta}$) is plotted in Fig. 8 which shows that the predicted L's from the 25 simulation runs lie close to a one-dimensional curve, confirming a nearly one-dimensional mapping between the linear combination of the inputs $\mathbf{w}_{\boldsymbol{\theta}}^T\boldsymbol{\theta}$ and L. In this situation, the one-dimensional active direction is sufficient to describe the behavior of the flame lift-off length. In addition, the narrow scatter of the bootstrap replicates indicates that 25 samples with the oversampling factor being 5 is sufficiently large for the SDR input space spanned by $\boldsymbol{\theta}$.

As shown in Fig. 7, L is significantly sensitive to three of the five parameters i.e., $\tilde{R}, Sc_t, Pr_t$, whereas it is insensitive to $C_{\varepsilon 1}$ and c_{flow}. The critical importance of the chemical kinetics is consistent with the findings in a chemical explosive mode analysis for this flame [47] that the buildup and evolution of the OH and H radicals dominates the chemical explosive mixing layer ahead of the flame initiation. More specifically, due to the monotonous-rise trend in the SSP(L, $\mathbf{w}_{\boldsymbol{\theta}}^T\boldsymbol{\theta}$), the negative sign of $\tilde{R}$ component indicates that a larger reaction rate shifts the flame towards upstream, which is caused by a shorter resident time required for the autoignition of a more reactive mixture. Besides the kinetics, the significant sensitivity of L to turbulent transport parameters Pr_t and Sc_t implies that turbulent mixing is also important for flame stabilization. The turbulence thermal conductivity increases with decreasing Pr_t, leading to more heat loss and shifting the flame further downstream. On the contrary, decrease Sc_t enhances the turbulence mass mixing for the non-premixed flows, which accelerates the ignition process and, hence moves the flame towards upstream. The small value of the $C_{\varepsilon 1}$ component provides the evidence that the turbulence eddy itself has much less effects on the flame stabilization location than the kinetics as well as turbulence thermal and mass diffusivity. The component corresponding to c_{flow} is also relatively small. Figure 9 shows the streamwise HRR profiles for cases with different c_{flow}'s, illustrating that the onset of the HRR is almost same for all the cases, while the downstream rise and decline become moderate with decreasing c_{flow} due to the increasing finite rate chemistry effects. The relatively uniform distribution for cases with small c_{flow}'s is also observed in the contour plots of the intermedium species H. Therefore, c_{flow} has very little impact on the onset of the flame. Because L is defined by the location of HRR peak, smaller c_{flow} leads to a slightly larger L, which is consistent with the negative sign of c_{flow} component in Fig. 7.

3.2.2. Assessment of the active rate-constant

Due to the critical importance of kinetics, the behavior of the active rate-constant $\tilde{R}$ is further assessed through independently sampling rate-constants in a direct AS analysis. The input space is then spanned by the vector $\boldsymbol{\zeta} = [\xi_1, \ldots, \xi_{21}, \langle Sc_t\rangle, \langle Pr_t\rangle, \langle C_{\varepsilon 1}\ \rangle, \langle c_{flow}\rangle]^T \in \mathbb{R}^{25}$. With the oversam-

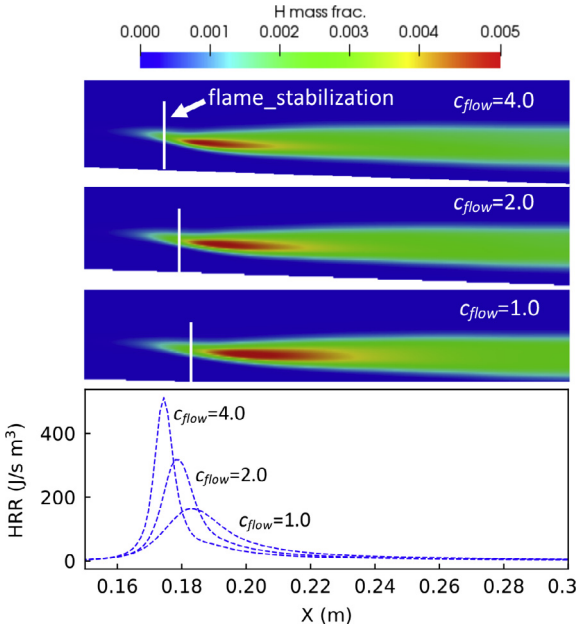

Fig. 9. The streamwise HRR profiles along the upper lip-line of fuel inlet, and H mass fraction contours for cases with c_{flow} of 1.0, 2.0 and 4.0.

pling factor being 2, $N = 50$ samples are drawn for $\boldsymbol{\zeta}$ according to the distribution densities. The components of the one-dimensional active subspace $\mathbf{w}_{\boldsymbol{\zeta}}$ are estimated with Algorithm 2.2 and shown in Fig. 10. The corresponding SSP(L,$\mathbf{w}_{\boldsymbol{\zeta}}^T\boldsymbol{\zeta}$) is plotted in Fig. 8, showing a reasonable univariate trend and the scatter is small even though larger than that of SSP(L, $\mathbf{w}_{\boldsymbol{\theta}}^T\boldsymbol{\theta}$) due to a lower oversampling factor. Nevertheless, the summary plot SSP(L,$\mathbf{w}_{\boldsymbol{\zeta}}^T\boldsymbol{\zeta}$) provide confidence of the one-dimensional active subspace $\mathbf{w}_{\boldsymbol{\zeta}}$, from which a equivalent active rate-constant, denoted by $\tilde{R}'$, can be obtained by computing the Euclidean norm of the vector that consists of all the kinetic components.

The equivalent $\tilde{R}'$ along with the physical components are plotted in Fig. 7 to make a comparison. As shown, $\tilde{R}$ from the SDR framework is consistent with that from direct AS analysis, further indicating that one can use a single active rate-constant instead of a large number of individual ones to account for the kinetic uncertainty in the UQ analysis for turbulent combustion simulations. It is also interesting to observe that, not only the kinetics is dominant as shown in Fig. 7, but the most important reaction R1 has the roughly same sensitivity as that of the most important turbulence parameter Pr_t as shown in Fig. 10. This suggests that to improve the confidence of L prediction, reducing the uncertainty in R1 is as important as reducing the uncertainty associated with turbulent heat diffusion. In other words, to reduce the uncertainty in the prediction and balance the error contributions from the models, the accuracy of the kinetic model, particularly the kinetic parameters of key reactions, e.g. R1, R3 and R9, needs substantial improvement, together with the careful calibration of the turbulent transport parameters. For the turbulence and combustion models employed in this study, the corresponding model parameters has negligible influence on the prediction uncertainty and no further improvement is needed.

3.2.3. Effects of physical parameter uncertainties on key reactions

From Fig. 10, the effects of the physical uncertainties on the key reactions can also be addressed through the comparison of $\mathbf{w}_{\boldsymbol{\zeta}}$ and $\mathbf{w}_{\boldsymbol{\xi},\mathbf{1}}$ from the B-K simulations. As shown, when the physical parameters are uncertain, the sensitivity of L to reaction R1 ($H + O_2 \leftrightharpoons O + OH$) is weaken while R9 ($H + O_2$ (+ M) $\leftrightharpoons HO_2$ (+ M)) and R11 ($HO_2 + H \leftrightharpoons OH + OH$) are significantly promoted. This is mainly caused by the local temperature change in the reaction zone due to the uncertainty in Pr_t which dominates physical effects among the four physical parameters. To confirm this claim and gain a better understanding, the rate-constants of R1 and R9 as a function of temperature are plotted in Fig. 11. Note that the chain-branching reactions R1 and the chain-propagating reaction R9 are competitive in consuming H and O_2. The rate-constant k_1 is in a modified Arrhenius form, i.e. $k_1(T) = AT^n\exp(-E_a/RT)$, while k_9 is a pressure-dependent falloff reaction and follows the expression

$$k_9(T) = k_\infty\left(\frac{P_r}{1+P_r}\right)F(P_r), \tag{9}$$

where $F(P_r)$ is the falloff function and estimated by using Troe's fitting [57] with F_{cent}, $P_r = k_0[\text{M}]/k_\infty$, and $[\text{M}] = \sum \varepsilon_s C_s$. C_s and ε_s are the concentration and collision efficiency of species s, respectively. All the parameters are from the Li-2004 mechanism, and the concentrations are from the B-K simulations.

As shown in Fig. 11, the curves of k_1 and k_9 intersect at the temperature of 1082 K, denoted by T_{critical}, below which R1 dominates the reaction between H and O_2, whereas when the temperature goes above T_{critical}, R1 rapidly overtakes R9. The value of T_{critical} is also marked in Fig. 3, from which it can be observed that the temperature at the flame stabilization location is around T_{critical}. This suggests that uncertainty associated with turbulent heat diffusion would induce uncertain local temperature randomly distributed around T_{critical}, leading to different dominant reaction regimes in the flame stabilization zone. Specifically, when Pr_t is assigned with the uncertainty range of [0.5, 1.0] which is the case in the present work, rather than the nominal value of 0.9, the local temperature is more likely to be below the nominal one, since heat diffusion is enhanced with decreasing Pr_t. This would subsequently increase the reaction rate of R9 while decrease that of R1, explaining when physical uncertainty is taken into account, the formation and consumption of HO_2 reactions are promoted and H_2/O_2 chain reactions are conversely inhibited as shown in Fig. 10.

3.3. Quantification of modeling uncertainties

The summary plots of SSP(L,$\mathbf{w}_{\boldsymbol{\xi},1}^T\boldsymbol{\xi}$) and SSP($L$,$\mathbf{w}_{\boldsymbol{\theta}}^T\boldsymbol{\theta}$), SSP($L$,$\mathbf{w}_{\boldsymbol{\zeta}}^T\boldsymbol{\zeta}$) in Figs. 7 and 9, respectively, indicate that univariate models are reasonable choices for propagating the corresponding input uncertainty. Therefore, based on second-order polynomial fitting, the response surfaces are constructed in the corresponding active subspaces as shown in Fig. 6 for only the kinetic uncertainties considered and Fig. 12a for both the kinetic and physical uncertainties considered, with and without SDR. The R-square values of the fitting for SSP(L,$\mathbf{w}_{\boldsymbol{\xi},1}^T\boldsymbol{\xi}$), SSP($L$,$\mathbf{w}_{\boldsymbol{\theta}}^T\boldsymbol{\theta}$) and SSP($L$,$\mathbf{w}_{\boldsymbol{\zeta}}^T\boldsymbol{\zeta}$) are 0.994, 0.986 and 0.982, respectively, confirming that the fitting error of the response surfaces is sufficiently small. Then the propagation of the kinetic uncertainties is first investigated based on the response surfaces, followed by the propagation of the kinetic-physical uncertainties.

3.3.1. Propagation of kinetic uncertainties

Figure 12b shows the PDFs of L estimated by drawing 10,000 samples. As shown, when only the kinetic uncertainties are taken into account to build the response surface, the mean of the uncertain L is 0.177 m and the 95% confidence interval is [0.124 m, 0.227 m]. When both the kinetic and physical uncertainties are included to construct the response surface, the mean of L is 0.207 and 0.216 m with and without SDR, respectively. The 95% confidence interval is [0.152 m, 0.265 m] and [0.152 m, 0.279 m] with and without SDR, respectively. The results show that the two sets of kinetic-introduced uncertainty of L are roughly consistent

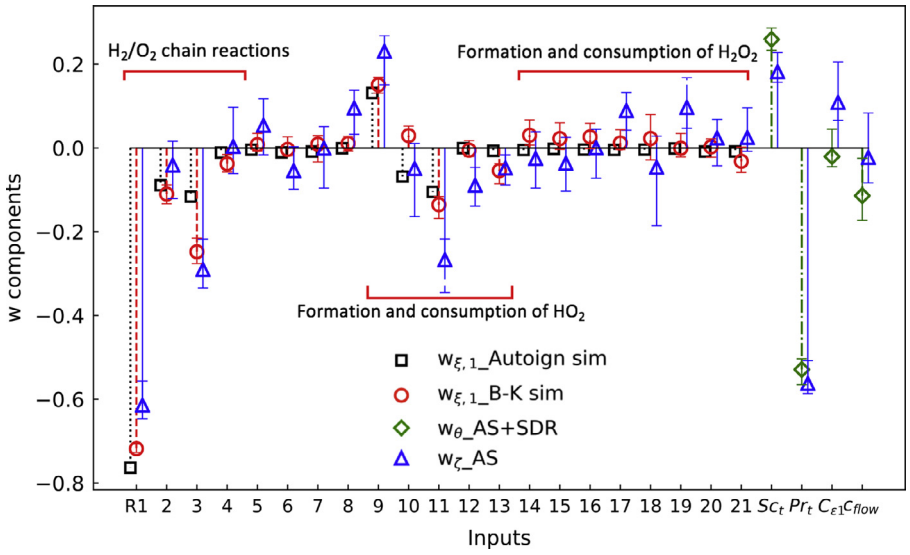

Fig. 10. The components of the B-K flame active subspace for flame lift-off length L with and without the SDR framework, also shown is the kinetics active subspace computed through autoignition simulations and B-K simulations.

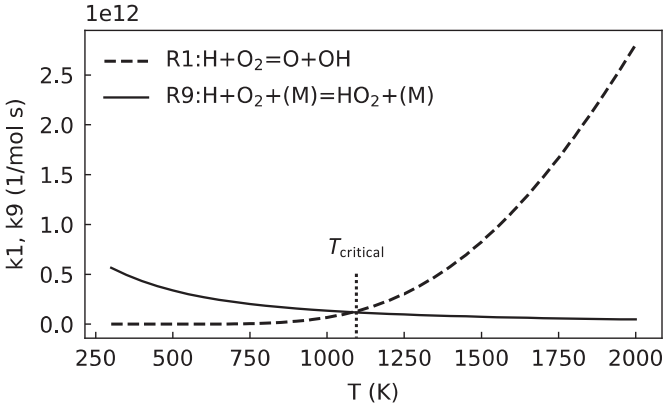

Fig. 11. Reaction rate-constants of the reaction R1 and R9 as a function of temperature.

whether or not they employ the SDR, indicating that the kinetic uncertainty can be properly propagated within the proposed SDR framework. More interestingly, the comparison between the PDFs with the legends of 'only kinetics' and 'SDR+AS' demonstrates that the physical uncertainty effects increase the mean of L while the length of the 95% confidence interval remains the same. This is consistent with the discussions in Section 3.2 that, the physical uncertainty effects promote the sensitivity to the reaction R9 which has a slower reaction rate than R1 and subsequently retard the autoignition process, ultimately resulting in a shift of the flame towards downstream.

3.3.2. Propagation of coupled physiochemical uncertainties

Based on the response surfaces in Fig. 12a, the kinetic and physical uncertainties are propagated to L through 10,000 times independently sampling the inputs of $\boldsymbol{\theta}$ within the SDR framework and $\boldsymbol{\zeta}$ with direct AS analysis. The resulting PDFs of L are shown in Fig. 13a. The mean of L is 0.209 and 0.217 m with and without SDR, respectively. The 95% confidence interval of L with SDR is [0.145 m, 0.276 m], which is slightly smaller than that estimated with direct AS analysis. Nevertheless, the comparison between the two PDFs of L indicates that the kinetic and physical parameter uncertainties can be properly propagated within the SDR framework, validating the proposed SDR framework in the current application.

Moreover, the PDFs considering only the kinetic uncertainty $\widetilde{R}$ and only the physical uncertainties, i.e., Sc_t, Pr_t, $C_{\varepsilon 1}$ and c_{flow} are evaluated based on the SDR response surface in Fig. 12a. As shown in Fig. 13b, these two PDFs are essentially overlapped, indicating that the uncertainty of L introduced by the physical parameter uncertainties, particularly by turbulence mass and heat diffusion as discussed in Section 3.2, is comparable with that introduced by the

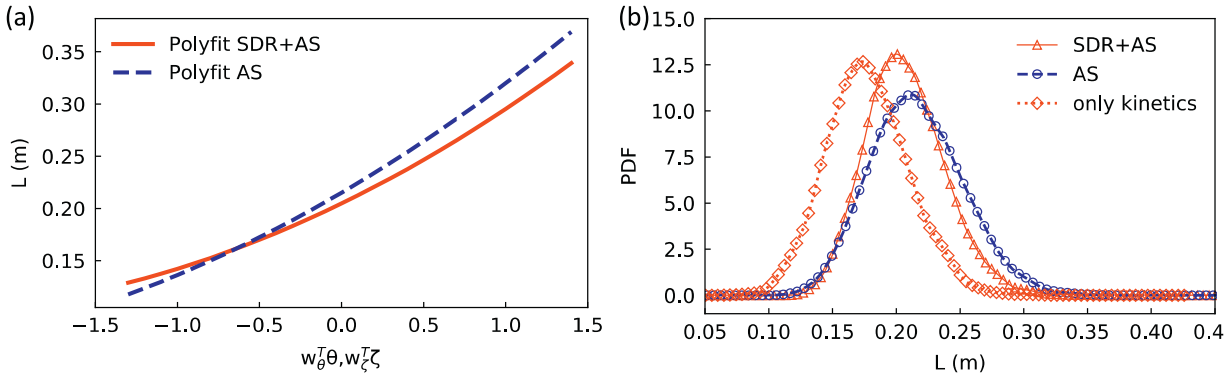

Fig. 12. (a) The response surfaces constructed in the active subspaces by fitting SSP(L,$\mathbf{w}_{\boldsymbol{\theta}}^T\boldsymbol{\theta}$) within the SDR framework and SSP(L,$\mathbf{w}_{\boldsymbol{\zeta}}^T\boldsymbol{\zeta}$) in direct AS analysis; and (b) the PDFs of L evaluated based on the response surfaces with 10,000 samples.

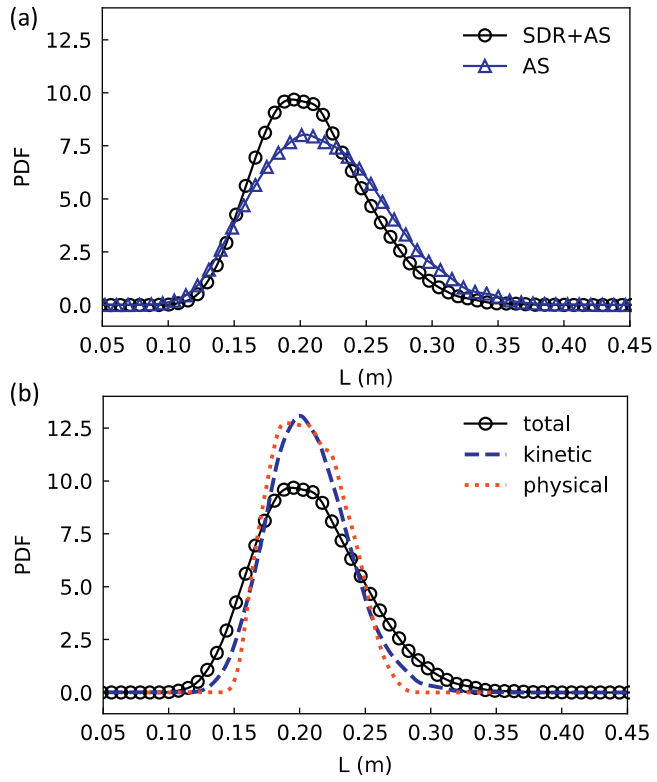

Fig. 13. The PDF of the flame lift-off length within the SDR framework along with the comparison to (a) the PDF with direct AS analysis and (b) the PDFs separately introduced by kinetics and turbulence.

kinetic uncertainty, even though the kinetics is dominant in L prediction. This result suggests that in addition to the kinetic uncertainty, one should also sufficiently consider uncertainty associated with turbulence and combustion models to improve the confidence in the prediction of the turbulent flames, even though the dominant role of the kinetics on the flame lift-off length has been well proved in this application.

4. Conclusions

In this work, a successive dimension reduction (SDR) framework based on the active subspace (AS) method is formulated to reduce the dimension of the physiochemical uncertainty space for modeling uncertainty quantification of turbulent flames. The performance of the SDR framework is demonstrated with the Burrows–Kurkov (B–K) wall-jet flame simulations which consider 21 uncertain rate-constants, and four physical uncertainty parameters, i.e. Sc_t, Pr_t, $C_{\varepsilon 1}$ and c_{flow}. A one-dimensional active subspace and the corresponding single active rate-constant are identified for the 21 rate-constants through the cheap surrogate autoignition simulations. The dimension of the reconstructed input space including uncertain physical parameters and the active rate-constant is reduced to one, enabling efficient UQ of the predicted flame lift-off length through the response surface built in this one-dimensional subspace. In addition, the dimension of the uncertainty space is also reduced through direct AS analysis to assess the SDR framework.

The active subspaces of the uncertain rate-constants computed though the autoignition tests and B-K simulations are essentially the same, indicating the zero-D autoignition tests are able to surrogate the expensive B-K simulations to identify the active subspace for the kinetics. The components of the active subspace reveal that the chain branching reaction R1 ($H+O_2 \leftrightharpoons O+OH$) dominates the ignition delay time as well as the flame lift-off length. Further comparison between the active rate-constant and the equivalent one from the B-K simulations, confirms the ability of the active rate-constant in propagating the kinetic uncertainties when the physical uncertainties are also considered. From the comparison between the PDFs from the SDR framework and direct AS analysis, it is concluded that the SDR framework can reproduce the probability distribution of the predicted flame lift-off length driven from kinetic and physical parameter uncertainties.

The physical uncertainties, particularly the uncertainty associated with turbulent heat diffusion, is found to have impact on the kinetic uncertainties propagation through promoting the reactions of formation and consumption of HO_2, particularly reactions R9 ($H+O_2$ (+M) $\leftrightharpoons$ HO_2 (+M)) and R11 ($HO_2+H \leftrightharpoons OH+OH$), and weaken the H_2/O_2 chain reactions, mainly R1. The uncertainty in the turbulent heat diffusion introduces the variation of the local temperature in the flame stabilization zone and subsequently changes the dominant reaction between the competitive reactions R1 and R9. A more prevalent role of R9 retards the autoignition and leads to a larger mean of the flame lift-off length than that without the physical uncertainty.

The components of the active subspace reveal that chemical kinetics plays a dominant role for the flame stabilization location, followed by turbulent transport parameters Pr_t and Sc_t, whereas the turbulence and combustion model parameters $C_{\varepsilon 1}$ and c_{flow} have negligible impact on L. The PDFs of L further show that the uncertainty induced by chemical kinetics is comparable with that induced by the overall physical models. Both chemical kinetics and turbulent mixing are essential for the flame initiation in the B-K flame. Note that current work considers only the uncertainties in model parameters, future work may include the quantification of model-form uncertainty.

Declaration of Competing Interest

Manuscript title: Quantification of modeling uncertainties in turbulent flames through successive dimension reduction

The authors whose names are listed immediately below certify that they have NO affiliations with or involvement in any organization or entity with any financial interest (such as honoraria; educational grants; participation in speakers' bureaus; membership, employment, consultancies, stock ownership, or other equity interest; and expert testimony or patent-licensing arrangements), or non-financial interest (such as personal or professional relationships, affiliations, knowledge or beliefs) in the subject matter or materials discussed in this manuscript.

Acknowledgments

This work was supported by the National Natural Science Foundation of China No. 91841302, National Science and Technology Major Project (2017-I-0004-0005), and China Postdoctoral Science Foundation (2020M670323).

Appendix A. Governing equations and numerical details of Burrows–Kurkov flame simulations

The computational model solves the Reynolds averaged Naiver-Stokes equations for compressible reacting flows. The total fluid density equation, continuity equation for species m, momentum equation and energy equation are

$$\frac{\partial \bar{\rho}}{\partial t} + \frac{\partial \bar{\rho}\tilde{u}_j}{\partial x_j} = 0, \tag{A1}$$

$$\frac{\partial \bar{\rho}\tilde{Y}_s}{\partial t}+\frac{\partial \bar{\rho}\tilde{Y}_s\tilde{u}_j}{\partial x_j}=\frac{\partial}{\partial x_j}\left(\bar{\rho}D_s\frac{\partial \tilde{Y}_s}{\partial x_j}+\bar{\tau}^t_{\tilde{\emptyset}}\right)+\bar{\dot{\omega}}_s, s=1,\ 2,\ldots,\ ns-1, \tag{A2}$$

$$\frac{\partial \bar{\rho}\tilde{u}_i}{\partial t}+\frac{\partial \bar{\rho}\tilde{u}_i\tilde{u}_j}{\partial x_j}=-\frac{\partial \bar{p}}{\partial x_i}+\frac{\partial}{\partial x_j}\left(\bar{\tau}_{ij}+\bar{\tau}^t_{ij}\right), i=1,\ 2,\ 3, \tag{A3}$$

and

$$\frac{\partial \bar{\rho}\tilde{E}}{\partial t}+\frac{\partial \bar{\rho}\tilde{H}\tilde{u}_j}{\partial x_j}=\frac{\partial}{\partial x_j}\left[\kappa\frac{\partial \tilde{T}}{\partial x_j}+\sum_{s=1}^{ns}\left(\bar{\rho}D_s\tilde{h}_s\frac{\partial \tilde{Y}_s}{\partial x_j}\right)+\tilde{u}_i\bar{\tau}_{ij}+\bar{\tau}^t_{\tilde{e}}\right], \tag{A4}$$

respectively, where ρ is the mass density, u is the fluid velocity, Y is the mass fraction of species, D is the diffusion coefficient, $\tau^t{}_{ij}$ is the Reynolds stress tensor, $\dot{\omega}$ is the species mass production rate, p is the pressure, H is the total enthalpy, T is the temperature, h is the static enthalpy, i.e. the sum of the sensible and formation enthalpy. The superscripts ¯ and ˜ denote Reynolds averaged quantities and Favre averaged quantities, respectively. The subscript s denotes the quantities of species s. The thermal conductivity κ is a summation of two parts, i.e. the molecular one κ_m and the turbulent thermal conductivity κ_t, where $\kappa_t=\mu_t c_p\rho/Pr_t$ and μ_t is the turbulent viscosity. The molecular thermal conductivity κ_m is mixture-averaged through the mixing rule in the combination averaging formula [58]. The viscous stress tensor τ_{ij} is

$$\tau_{ij}=2\mu S_{ij}-\frac{2}{3}\mu S_{kk}\delta_{ij}, \tag{A5}$$

where μ is the molecular coefficient of viscosity, S_{ij} is the strain rate tensor and δ_{ij} is the Kronecker operator. The mixing rule for viscosity μ uses the Wilke semi-empirical formula [59]. For μ of each species, the Sutherland formula is used

$$\mu=\frac{A_s T^{3/2}}{T+T_s}, \tag{A6}$$

where A_s and T_s are constants.

The caloric equation of state for the enthalpy h of the gas mixture is

$$h=\sum_{s=1}^{ns}Y_s h_s,\ \ s=1,\ldots,ns, \tag{A7}$$

$$h_s=\Delta h^0_{f,s}+\int_{T_{std}}^{T}c_p dT \tag{A8}$$

where c_p is the specific heat capacity at constant pressure and Δh^0_f is the enthalpy of formation at the reference temperature T_{std}. E is the total energy expressed as

$$\tilde{E}=\sum_{s=1}^{ns}\left(\tilde{Y}_s\tilde{h}_s+\frac{1}{2}\tilde{u}_j\tilde{u}_j+k-\frac{\bar{p}}{\bar{\rho}}\right), \tag{A9}$$

where k is the turbulence kinetic energy. The equation of state for the gas mixture is

$$\bar{p}=\bar{\rho}\tilde{T}R\sum_{s=1}^{ns}\frac{\tilde{Y}_s}{M_s}, \tag{A10}$$

where R is the gas constant and M_s is the molecular weight of the species s.

Reynolds stress tensor $\bar{\tau}^t_{ij}$ is closed with the standard k-ε model together with the turbulent eddy viscosity assumption

$$\bar{\tau}^t_{ij}=2\mu_t\tilde{S}_{ij}-\frac{2}{3}\mu_t\tilde{S}_{kk}\delta_{ij}-\frac{2}{3}\bar{\rho}k\delta_{ij}. \tag{A11}$$

The governing equations for μ_t, k and its dissipation ε are

$$\mu_t=c_\mu\rho\frac{k^2}{\varepsilon}, \tag{A12}$$

$$\frac{\partial(\bar{\rho}k)}{\partial t}+\frac{\partial\left(\bar{\rho}\tilde{u}_j k\right)}{\partial x_j}=\tau_{ij}\frac{\partial\tilde{u}_i}{\partial x_j}-\bar{\rho}\varepsilon+\frac{\partial}{\partial x_j}\left[\left(\frac{\mu}{\mathrm{Pr}_k}\right)\frac{\partial k}{\partial x_j}\right], \tag{A13}$$

and

$$\frac{\partial(\bar{\rho}\varepsilon)}{\partial t}+\frac{\partial\left(\bar{\rho}\tilde{u}_j\varepsilon\right)}{\partial x_j}=\left(C_{\varepsilon1}\tau_{ij}\frac{\partial\tilde{u}_i}{\partial x_j}-C_{\varepsilon2}\bar{\rho}\varepsilon\right)\frac{\varepsilon}{k}+\frac{\partial}{\partial x_j}\left[\left(\frac{\mu}{\mathrm{Pr}_\varepsilon}\right)\frac{\partial\varepsilon}{\partial x_j}\right]+C_{\varepsilon3}\bar{\rho}\varepsilon\frac{\partial\tilde{u}_j}{\partial x_j}, \tag{A14}$$

where $C_{\varepsilon1}$, $C_{\varepsilon2}$, $C_{\varepsilon3}$, Pr_k, Pr_ε and c_μ are model constants given by values of 1.44, 1.92, −0.33, 1.0, 1.3 and 0.09, respectively. Turbulent heat-flux and diffusion terms are closed based on Simple Gradient Diffusion Hypothesis with turbulent Prandtl number Pr_t and turbulent Schmidt number Sc_t being 0.9 and 0.6, respectively as nominal values. For combustion, a finite-rate chemistry model, i.e. Partially Stirred Reactor (PaSR) model is adopted to handle autoignition and different modes of combustion. The sub-grid reaction rate $\bar{\dot{\omega}}$ is treated on a sub-grid level by scaling the resolved reaction rate $\dot{\omega}$ with a factor of $\tau_c/(\tau_c+\tau_{mix})$, i.e., $\bar{\dot{\omega}}=\tau_c\dot{\omega}/(\tau_c+\tau_{mix})$, where τ_c and τ_{mix} are chemical reaction time scale and turbulent mixing time scale, respectively. Here turbulent mixing time scale is modelled as $\tau_{mix}=k/(\varepsilon c_{flow})$, where c_{flow} is the turbulent rate constant of 4.0 as a nominal value. The detailed mechanism employed is the Li mechanism [48], which consists of 9 species (H_2, H, O, OH, O_2, N_2, H_2O, HO_2, H_2O_2) and 21 elementary reactions, including H_2/O_2 chain reactions, H_2/O_2 dissociation/recombination reactions, as well as formation and consumption of HO_2 and H_2O_2. The mechanism has been validated by experimental data from laminar premixed flames, shock tubes and flow reactors over a wide range (298–3000 K, 0.03–8.7 MPa, equivalence ratio $\emptyset$ = 0.25–5.0) [48].

All the simulations are performed over a two-dimensional (2-D) computational domain (see the dashed-line region in Fig. 1) with a one-cell-width 3-D mesh. The constant of 0.51 m of the combustor width (normal to the plane of drawing in Fig. 1) makes the 2-D simplification adequate in the simulations for cost-saving consideration. The inflow tunnel extends 0.2 m upstream. The inflow conditions are the same as those in the experiments listed in Table 1. The isothermal wall condition with a temperature of 300 K is set for all the wall boundaries. The wall-function boundary conditions are adopted to bridge the inner region between the wall and the main flow. The wall distance for the first cell is set to be 0.05 mm to guarantee the first cell center is in the log-law region. Four sets of structured grids are tested to achieve grid convergence by measuring the predicted error of the flame lift-off length. As shown in Fig. A1, the grid size of 0.4 mm in the mixing layer is sufficient to ensure less than 1% error, an equivalent 2 mm in lift-off length, which is substantially less than the uncertainty, i.e., 131 mm, associated with model parameters. Hence this set of grid is used in this study.

The governing equations are solved by a density-based solver based on the fully compressible flow solver *rhoCentralFoam* in OpenFOAM®. The inviscid flux vectors are discretized using the second-order Monotone Upstream-centered Scheme for Conservation Laws (MUSCL) method [60]. The Kurganov and Tadmor scheme [61] is adopted to capture the shocks. The viscous flux vectors are discretized using the central difference scheme. The time integration of the species governing equations is separated into chemical reaction sub-steps and transport sub-steps based on the splitting schemes [62]. The stiff ordinary differential equation (ODE) system in chemical reaction sub-steps, which is an initial value problem with given initial species mass fractions and temperature, is solved using the OpenFOAM built-in ODE solver. The time integration in

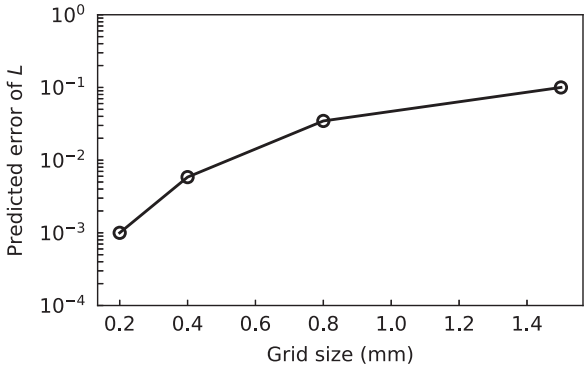

Fig. A1. The predicted errors of the flame lift-off length as the function of the grid size in the mixing layer.

transport sub-steps uses the preconditioned bi-conjugate gradient (PBiCG) method [63,64].

References

[1] H. Wang, D.A. Sheen, Combustion kinetic model uncertainty quantification, propagation and minimization, Prog. Energy Combust. Sci. 47 (2015) 1–31.
[2] M. Khalil, G. Lacaze, J.C. Oefelein, H.N. Najm, Uncertainty quantification in LES of a turbulent bluff-body stabilized flame, Proc. Combust. Inst. 35 (2015) 1147–1156.
[3] M.E. Mueller, G. Iaccarino, H. Pitsch, Chemical kinetic uncertainty quantification for Large Eddy Simulation of turbulent nonpremixed combustion, Proc. Combust. Inst. 34 (2013) 1299–1306.
[4] M.E. Mueller, V. Raman, Effects of turbulent combustion modeling errors on soot evolution in a turbulent nonpremixed jet flame, Combust. Flame 161 (2014) 1842–1848.
[5] M.E. Mueller, V. Raman, Model form uncertainty quantification in turbulent combustion simulations: peer models, Combust. Flame 187 (2018) 137–146.
[6] M.T. Reagan, H.N. Najm, R.G. Ghanem, O.M. Knio, Uncertainty quantification in reacting-flow simulations through non-intrusive spectral projection, Combust. Flame 132 (2003) 545–555.
[7] M.T. Reagan, H.N. Najm, P.P. Pébay, O.M. Knio, R.G. Ghanem, Quantifying uncertainty in chemical systems modeling, Int. J. Chem. Kinet. 37 (2005) 368–382.
[8] I.G. Zsély, J. Zádor, T. Turányi, Uncertainty analysis of updated hydrogen and carbon monoxide oxidation mechanisms, Proc. Combust. Inst. 30 (2005) 1273–1281.
[9] D.A. Sheen, X. You, H. Wang, T. Løvås, Spectral uncertainty quantification, propagation and optimization of a detailed kinetic model for ethylene combustion, Proc. Combust. Inst. 32 (2009) 535–542.
[10] D.A. Sheen, H. Wang, The method of uncertainty quantification and minimization using polynomial chaos expansions, Combust. Flame 158 (2011) 2358–2374.
[11] B.D. Phenix, J.L. Dinaro, M.A. Tatang, J.W. Tester, J.B. Howard, G.J. McRae, Incorporation of parametric uncertainty into complex kinetic mechanisms: application to hydrogen oxidation in supercritical water, Combust. Flame 112 (1998) 132–146.
[12] M. Reagan, H. Najm, B. Debusschere, O. Le Maître, O. Knio, R. Ghanem, Spectral stochastic uncertainty quantification in chemical systems, Combust. Theory Model. 8 (2004) 607–632.
[13] S.J. Klippenstein, L.B. Harding, M.J. Davis, A.S. Tomlin, R.T. Skodje, Uncertainty driven theoretical kinetics studies for CH_3OH ignition: HO_2+CH_3OH and O2+CH3OH, Proc. Combust. Inst. 33 (2011) 351–357.
[14] S.G. Davis, A.B. Mhadeshwar, D.G. Vlachos, H. Wang, A new approach to response surface development for detailed gas-phase and surface reaction kinetic model optimization, Int. J. Chem. Kinet. 36 (2004) 94–106.
[15] S. Li, B. Yang, F. Qi, Accelerate global sensitivity analysis using artificial neural network algorithm: case studies for combustion kinetic model, Combust. Flame 168 (2016) 53–64.
[16] P.R. Conrad, Y.M. Marzouk, Adaptive smolyak pseudospectral approximations, SIAM J. Sci. Comput. 35 (2013) A2643–A2670.
[17] A.S. Tomlin, E. Agbro, V. Nevrlý, J. Dlabka, M. Vašinek, Evaluation of combustion mechanisms using global uncertainty and sensitivity analyses: a case study for low-temperature dimethyl ether oxidation, Int. J. Chem. Kinet. 46 (2014) 662–682.
[18] G. Esposito, B.G. Sarnacki, H.K. Chelliah, Uncertainty propagation of chemical kinetics parameters and binary diffusion coefficients in predicting extinction limits of hydrogen/oxygen/nitrogen non-premixed flames, Combust. Theory Model. 16 (2012) 1029–1052.
[19] É. Hébrard, A.S. Tomlin, R. Bounaceur, F. Battin-Leclerc, Determining predictive uncertainties and global sensitivities for large parameter systems: a case study for n-butane oxidation, Proc. Combust. Inst. 35 (2015) 607–616.
[20] M. Frenklach, H. Wang, M.J. Rabinowitz, Optimization and analysis of large chemical kinetic mechanisms using the solution mapping method—Combustion of methane, Prog. Energy Combust. Sci. 18 (1992) 47–73.
[21] T.M. Russi, Uncertainty Quantification With Experimental Data and Complex System Models, UC Berkeley, 2010.
[22] P.G. Constantine, E. Dow, Q. Wang, Active subspace methods in theory and practice: applications to Kriging surfaces, SIAM J. Sci. Comput. 36 (2014) A1500–A1524.
[23] P.G. Constantine, Active Subspaces: Emerging Ideas for Dimension Reduction in Parameter Studies, SIAM, Philadelphia, 2015.
[24] P.G. Constantine, M. Emory, J. Larsson, G. Iaccarino, Exploiting active subspaces to quantify uncertainty in the numerical simulation of the HyShot II scramjet, J. Comput. Phys. 302 (2015) 1–20.
[25] K. Pearson LIII, On lines and planes of closest fit to systems of points in space, Lond. Edinb. Dublin Philos. Mag. J. Sci. 2 (1901) 559–572.
[26] J.A. Beck, J.M. Brown, A.A. Kaszynski, E.B. Carper, Active Subspace Development of Integrally Bladed Disk Dynamic Properties Due to Manufacturing Variations, J Eng Gas Turbine Power (2018) 141.
[27] Z. del Rosario, P. Constantine, G. Iaccarino, Developing design insight through active subspaces, 19th AIAA Non-Deterministic Approaches Conference, 2017.
[28] Z.J. Grey, P.G. Constantine, Active subspaces of airfoil shape parameterizations, AIAA J. 56 (2018) 2003–2017.
[29] P. Seshadri, S. Shahpar, P. Constantine, G. Parks, M. Adams, Turbomachinery active subspace performance maps, J. Turbomach. 140 (2018).
[30] A.F. Cortesi, P.G. Constantine, T.E. Magin, P.M. Congedo, Forward and backward uncertainty quantification with active subspaces: application to hypersonic flows around a cylinder, J. Comput. Phys. 407 (2020) 109079.
[31] W. Ji, J. Wang, O. Zahm, Y.M. Marzouk, B. Yang, Z. Ren, C.K. Law, Shared low-dimensional subspaces for propagating kinetic uncertainty to multiple outputs, Combust. Flame 190 (2018) 146–157.
[32] W. Ji, Z. Ren, Y. Marzouk, C.K. Law, Quantifying kinetic uncertainty in turbulent combustion simulations using active subspaces, Proc. Combust. Inst. 37 (2019) 2175–2182.
[33] R. Cabra, T. Myhrvold, J.Y. Chen, R.W. Dibble, A.N. Karpetis, R.S. Barlow, Simultaneous laser raman-rayleigh-lif measurements and numerical modeling results of a lifted turbulent H2/N2 jet flame in a vitiated coflow, Proc. Combust. Inst. 29 (2002) 1881–1888.
[34] M. Vohra, A. Alexanderian, H. Guy, S. Mahadevan, Active subspace-based dimension reduction for chemical kinetics applications with epistemic uncertainty, Combust. Flame 204 (2019) 152–161.
[35] M. Burrows, A. Kurkov, Supersonic combustion of hydrogen in a vitiated air stream using stepped-wall injection, 7th Propulsion Joint Specialist Conference (1971), p. 721.
[36] M.C. Burrows, A.P. Kurkov, An analytical and experimental study of supersonic combustion of hydrogen in vitiated air stream, AIAA J. 11 (1973) 1217–1218.
[37] V. Gururajan, F.N. Egolfopoulos, Direct sensitivity analysis for ignition delay times, Combust. Flame 209 (2019) 478–480.
[38] C. Guan, J. Zhai, D. Han, Cetane number prediction for hydrocarbons from molecular structural descriptors based on active subspace methodology, Fuel 249 (2019) 1–7.
[39] P.G. Constantine, B. Zaharatos, M. Campanelli, Discovering an active subspace in a single-diode solar cell model, Stat. Anal. Data Min. 8 (2015) 264–273.
[40] M. Vohra, S. Mahadevan, Discovering the active subspace for efficient UQ of molecular dynamics simulations of phonon transport in silicon, Int J Heat Mass Transf. 132 (2019) 577–586.
[41] R.D. Cook, Regression Graphics: Ideas for Studying Regressions Through Graphics, John Wiley & Sons, 2009.
[42] B. Efron, R.J. Tibshirani, An Introduction to the Bootstrap, CRC press, 1994.
[43] P.G. Constantine, P. Diaz, Global sensitivity metrics from active subspaces, Reliab. Eng. Syst. Saf. 162 (2017) 1–13.
[44] Z. Luo, C.S. Yoo, E.S. Richardson, J.H. Chen, C.K. Law, T. Lu, Chemical explosive mode analysis for a turbulent lifted ethylene jet flame in highly-heated coflow, Combust. Flame 159 (2012) 265–274.
[45] H. Wang, S.B. Pope, Lagrangian investigation of local extinction, re-ignition and auto-ignition in turbulent flames, Combust. Theory Model. 12 (2008) 857–882.
[46] H. Wang, H. Zhou, Z. Ren, C.K. Law, Transported PDF simulation of turbulent CH_4/H_2 flames under MILD conditions with particle-level sensitivity analysis, Proc. Combust. Inst. 37 (2019) 4487–4495.
[47] W. Wu, Y. Piao, H. Liu, Analysis of flame stabilization mechanism in a hydrogen-fueled reacting wall-jet flame, Int. J. Hydrogen Energy 44 (2019) 26609–26623.
[48] J. Li, Z. Zhao, A. Kazakov, F.L. Dryer, An updated comprehensive kinetic model of hydrogen combustion, Int. J. Chem. Kinet. 36 (2004) 566–575.
[49] M.T. Reagan, H.N. Najm, B.J. Debusschere, O.P. Le Maître, O.M. Knio, R.G. Ghanem, Spectral stochastic uncertainty quantification in chemical systems, Combust. Theory Model. 8 (2004) 607–632.
[50] A.A. Konnov, Remaining uncertainties in the kinetic mechanism of hydrogen combustion, Combust. Flame 152 (2008) 507–528.
[51] E.T. Jaynes, Information theory and statistical mechanics. II, Phys. Rev. 108 (1957) 171.
[52] S.B. Pope, An explanation of the turbulent round-jet/plane-jet anomaly, AIAA J. 16 (1978) 279–281.
[53] X. Xiao, J.R. Edwards, H.A. Hassan, A.D. Culter, Variable turbulent Schmidt-number formulation for scramjet applications, AIAA J. 44 (2006) 593–599.

[54] D. Eklund, R. Baurle, M. Gruber, Numerical study of a scramjet combustor fueled by an aerodynamic ramp injector in dual-mode combustion, 39th Aerospace Sciences Meeting and Exhibit (2001), p. 379.
[55] W. Wu, Y. Piao, Q. Xie, Z. Ren, Flame diagnostics with a conservative representation of chemical explosive mode analysis, AIAA J. 57 (2019) 1355–1363.
[56] D. Goodwin, An open-source, extensible software suite for CVD process simulation, Chem. Vapor Deposition XVI EUROCVD 14 (2003) 2003–2008.
[57] J. Troe, Predictive possibilities of unimolecular rate theory, J. Phys. Chem. 83 (1979) 114–126.
[58] S. Mathur, P. Tondon, S. Saxena, Thermal conductivity of binary, ternary and quaternary mixtures of rare gases, Mol. Phys. 12 (1967) 569–579.
[59] C. Wilke, A viscosity equation for gas mixtures, J. Chem. Phys. 18 (1950) 517–519.
[60] B. van Leer, Towards the ultimate conservative difference scheme. II. Monotonicity and conservation combined in a second-order scheme, J. Comput. Phys. 14 (1974) 361–370.
[61] A. Kurganov, E. Tadmor, New high-resolution central schemes for nonlinear conservation laws and convection–diffusion equations, J. Comput. Phys. 160 (2000) 241–282.
[62] Z. Ren, C. Xu, T. Lu, M.A. Singer, Dynamic adaptive chemistry with operator splitting schemes for reactive flow simulations, J. Comput. Phys. 263 (2014) 19–36.
[63] Y. Saad, H.A. Van Der Vorst, Iterative solution of linear systems in the 20th century, J. Comput. Appl. Math. 123 (2000) 1–33.
[64] Z. Mikić, E.C. Morse, The use of a preconditioned bi-conjugate gradient method for hybrid plasma stability analysis, J. Comput. Phys. 61 (1985) 154–185.